Inorganic Chemistry

ARTICLE

pubs.acs.org/IC

Combined Experimental and Theoretical Study on Redox-Active d^8 Metal Dithione−Dithiolato Complexes Showing Molecular Second-Order Nonlinear Optical Activity

Luca Pilia,[†] Davide Espa,[†] Alberto Barsella,[‡] Alain Fort,[‡] Christodoulos Makedonas,[§] Luciano Marchiò,[∥] Maria Laura Mercuri,[†] Angela Serpe,[†] Christiana A. Mitsopoulou,[§,*] and Paola Deplano*[,†]

[†]Dipartimento di Chimica Inorganica ed Analitica, Università di Cagliari, I-09042 Monserrato (Cagliari) Italy

[‡]Département d'Optique ultra-rapide et Nanophotonique, IPCMS-CNRS, 23 Rue du Loess, BP 43, 67034 Strasbourg Cedex 2, France

[§]Chemistry Department, Inorganic Laboratory, University of Athens, Panepistimiopolis, Zografou 15 771, Greece

[∥]Dipartimento di Chimica Generale ed Inorganica, Chimica Analitica, Chimica Fisica, Università di Parma, Parco Area delle Scienze 17A, I43100 Parma, Italy

Supporting Information

ABSTRACT: Synthesis, characterization, NLO properties, and theoretical studies of the mixed-ligand dithiolene complexes of the nickel triad [M(II)(Bz_2pipdt)(mnt)] (Bz_2pipdt = 1,4-dibenzyl-piperazine-3,2-dithione, mnt = maleonitriledithiolato, M(II) = Ni, **1**, Pd, **2**, Pt, **3**) are reported. Molecular structural characterization of **1**−**3** points out that four sulfur atoms are in a slightly distorted square-planar geometry. While the M−S bond distances are only slightly different, comparison of the C−C and C−S bonds in the $C_2S_2MS_2C_2$ core allows us to point out a significant difference between the C−C and the C−S distances in Bz_2pipdt and mnt. These findings suggest assigning a dithiolato character to mnt (*pull* ligand) and a dithione one (*push* ligand) to Bz_2pipdt. Cyclic voltammetry of **1**−**3** exhibits two reversible reduction waves and a broad irreversible oxidation wave. These complexes are characterized in the visible region by a peak of moderately strong intensity, which undergoes negative solvatochromism. The molecular quadratic optical nonlinearities were determined by the EFISH technique, which provided the following values $\mu\beta_\lambda$ (10^{-48} esu) = −1436 (**1**), −1450 (**2**), and −1950 (**3**) converted in $\mu\beta_0$ (10^{-48} esu) = −463 (**1**), −684 (**2**), and −822 (**3**), showing that these complexes exhibit large negative second-order polarizabilities whose values depend on the metal, being highest for the Pt compound. DFT and TD-DFT calculations on **1**−**3** allow us to correlate geometries and electronic structures. Moreover, the first molecular hyperpolarizabilities have been calculated, and the results obtained support that the most appealing candidate as a second-order NLO chromophore is the platinum compound. This is due to (i) the most extensive mixture of the dithione/metal/dithiolato orbitals, (ii) the influence of the electric field of the solvent on the frontier orbitals that maximizes the difference in dipole moments between the excited and the ground state, and (iii) the largest oscillator strength in the platinum case vs nickel and palladium ones.

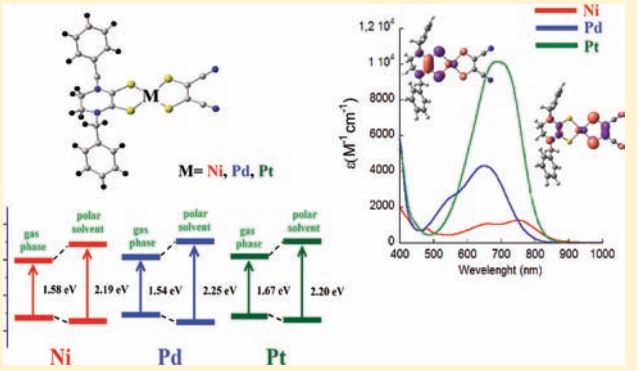

INTRODUCTION

Metal d^8 mixed-ligand dithiolenes based on two different dithiolene ligands [$R_2(C_2S_2)M(C_2S)R_2'$], each ligand bearing a different terminal group ($R \neq R'$) with significantly different electron-withdrawing capability, may behave as intervalence compounds where the ligand occurs in formally different oxidation states, as recognized by Vogler and Kunkely since the early 1980s.[1] Similar to what happens in the metal d^8 diimine−dithiolato complexes, in these mixed-ligand dithiolenes one ligand is reducing, dithiolato, *pull* ligand, which gives prevailing contribution to the HOMO a π orbital lying at high energy, and the other is oxidizing, dithione, *push* ligand, which gives prevailing contribution to the LUMO a π orbital lying at low energy.[2] Thus, the HOMO−LUMO transition will have ligand-to-ligand charge-transfer (CT) character mediated by the coordinated metal.

In Scheme 1, the structures A (X = S, dithione, or = N, diimine) and B depict qualitatively the limiting structures of the ground and excited state, respectively. Metal diimine−dithiolato complexes are known to behave as second-order nonlinear optical (NLO) chromophores,[2] and renewed interest in this class of compounds is related both to their applications in dye-sensitized solar cells[3] and to the photogeneration of H_2 from H_2O.[4]

Received: April 15, 2011
Published: September 22, 2011

Scheme 1

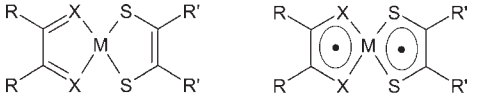

These complexes are characterized by an absorption band with medium to low molar absorption coefficients exhibiting large negative solvatochromism in the visible region of the spectrum. Theoretical calculations have confirmed the CT character of this peak related to the HOMO−LUMO transition and have shown that the HOMO is formed by a mixture of metal and dithiolato orbitals while the diimine orbitals give a predominant contribution to the LUMO. Accordingly, this transition has been termed mixed metal−ligand-to-ligand charge transfer, MMLL′CT.[5] The negative character of the solvatochromism of this peak and of the molecular first hyperpolarizability (β) value is determined by the fact that the charge-transfer axis is collinear but antiparallel to the ground-state dipole of the molecule, and thus, the excited state is predicted to be less polar than the ground state (see Scheme 1). The magnitude of the molecular first hyperpolarizability of several complexes, determined from electric-field-induced second-harmonic (EFISH) generation experiments at 1.9 μm, ranges from 0 to -39×10^{-30} esu.[2b] An optimized value as high as $\mu\beta_0 = -433 \times 10^{-48}$ esu, remarkably large for a metal complex, has been determined for a platinum derivative.[6]

Mixed-ligand dithiolene complexes are difficult to obtain in high yields and in pure form when the *push*−*pull* character of the ligands is similar since their formation often results in an equilibrium mixture of asymmetrical and symmetrical complexes, difficult to separate.[1]

After several attempts, nickel−mixed-ligand dithiolenes have been prepared in high yields using suitable ligands bearing substituents with significantly different *push*−*pull* character. In accordance with expectations, they exhibit negative solvatochromism and β comparable to or even higher than in the diimine−dithiolato cases.[7] When cationic and anionic complexes are available as starting reagents, their mixing provides a very effective method to prepare mixed-ligand complexes.[7b−d] While several stable anionic complexes are known, cationic dithiolenes are uncommon. Among these, the class of dicationic dithiolenes $[Ni(R_2pipdt)_2]^{2+}$ (R_2pipdt = 1,4-dialkyl-piperazine-3,2-dithione) have proved to be suitable precursors to prepare in almost quantitative yields mixed-ligand derivatives by reacting with Ni-anionic dithiolenes.[7b,c,8] However, this reaction does not work when the starting dications are palladium or platinum complexes in spite of nickel, as shown in Scheme 2a. In fact, $[M(R_2pipdt)_2][M(mnt)_2]$ (M = Pd and Pt; mnt = maleonitriledithiolato), double salts exhibiting ion-pair charge-transfer transitions, are obtained[9] in spite of the mixed-ligand complex $[Ni(R_2pipdt)(mnt)]$.

Fully characterized palladium and platinum mixed-ligand dithiolene complexes are still rare,[10] and to the best of our knowledge, no systematic studies have so far been performed on the second-order NLO activity inside the Ni triad combining experimental and theoretical studies to investigate the relevant factors and, in particular, the role of the metal in affecting the properties of the mixed-ligand complexes. After several attempts we succeeded in preparing in high yields mixed-ligand complexes of the Ni triad[11] using the new synthetic procedure shown in Scheme 2b.

Scheme 2

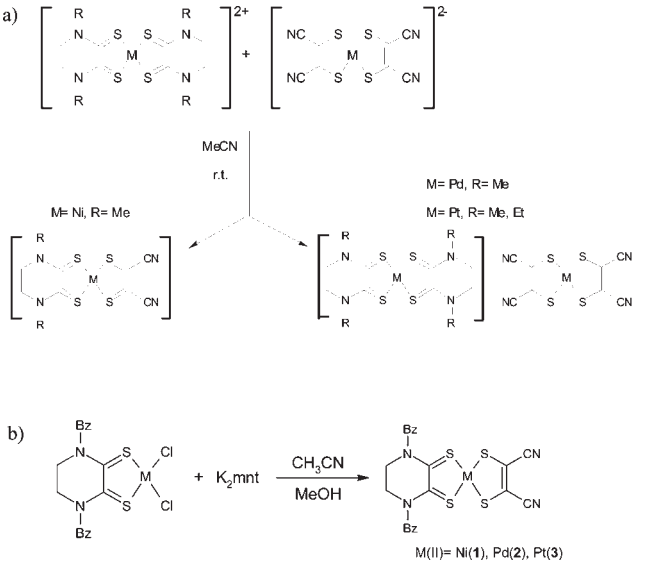

The synthesis and full characterization of the triad [M(II)-(Bz_2pipdt)(mnt)] (Bz = benzyl; M(II) = Ni, **1**, Pd, **2**, Pt, **3**), including second-order NLO properties, are reported here. This triad represents a case study suitable for a combined experimental and theoretical study to highlight the factors, in particular the role of the metal, which affect the properties of the complexes, with the view to optimize their quadratic NLO activity.

RESULTS AND DISCUSSION

$[Ni(Bz_2pipdt)(mnt)]$ (**1**) can be obtained as summarized in Scheme 2a. Dropwise addition of a THF solution of $[Ni(Bz_2pipdt)_2](BF_4)_2$ to a CH_3CN solution of $(Bu_4N)_2[Ni(mnt)_2]$ produces almost quantitatively **1**. On slow evaporation of the solvents, well-formed green crystals precipitated. These crystals are suitable for X-ray diffractometric characterization, which shows that **1** crystallizes in the monoclinic *C*2/*c* space group. This reaction using the corresponding M = Pd and Pt complexes does not afford the mixed-ligand dithiolenes but CT double salts, as shown in Scheme 2a. Preparation of all complexes of the triad in high yields has been obtained by reacting $[M(II)(Bz_2pipdt)Cl_2]$ with maleonitriledithiolato dianion. In fact, $[M(II)(Bz_2pipdt)Cl_2]$ are prepared by mixing, in CH_3CN under reflux, an equimolar amount of Bz_2pipdt and nickel dichloride, $[Pd(CH_3CN)_2Cl_2]$ and $[Pt(DMSO)_2Cl_2]$.[12] By reacting the maleonitriledithiolato dianion with $[M(II)(Bz_2pipdt)Cl_2]$, facile displacement of two chloride ions with the chelating mnt ligand is obtained according to Scheme 2b.

Crystals suitable for X-ray diffractometric studies have been obtained also for $[Pd(Bz_2pipdt)(mnt)]$ (**2**) and $[Pt(Bz_2pipdt)(mnt)]$ (**3**). The two compounds **2** and **3** are isostructural, and they crystallize in the orthorhombic *Pbcn* space group. Due to the isostructural nature of **2** and **3** only the molecular structure of the latter will be described in detail. A summary of X-ray crystallographic data and selected bond lengths and angles for all complexes are reported in Tables 1 and 2, while the molecular drawing of **1** is depicted in Figure 1. In all complexes, four sulfur atoms from two different ligands define the coordination environment of the metals, which are in a slightly distorted square planar geometry since the

dx.doi.org/10.1021/ic2007765 |*Inorg. Chem.* 2011, 50, 10015–10027

Table 1. Summary of X-ray Crystallographic Data for [M(II)(Bz$_2$pipdt)(mnt)] 1 (M = Ni), 2 (M = Pd), and 3 (M = Pt)[a]

	1	2	3
empirical formula	$C_{22}H_{18}N_4NiS_4$	$C_{22}H_{18}N_4PdS_4$	$C_{22}H_{18}N_4PtS_4$
fw	525.35	573.04	661.73
color, habit	black, prism	brown, prism	black, prism
crysta size, mm	0.25 × 0.10 × 0.05	0.45 × 0.15 × 0.10	0.45 × 0.15 × 0.10
cryst syst	monoclinic	orthorhombic	orthorhombic
space group	*C*2/c	*P*bcn	*P*bcn
a, Å	22.154(7)	21.414(2)	21.374(6)
b, Å	13.529(5)	13.705(1)	13.712(4)
c, Å	7.962(3)	8.073(1)	8.097(1)
α, deg	90	90	90
β, deg	106.73(2)	90	90
γ, deg	90	90	90
V, Å^3	2285(1)	2369.3(4)	2373(1)
Z	4	4	4
T, K	293(2)	293(2)	293(2)
ρ(calcd), Mg/m^3	1.527	1.607	1.852
μ, mm^{-1}	1.232	1.153	6.282
θ range, deg	1.79 to 26.00	1.76 to 27.03	1.76 to 27.08
no. of rflns/unique reflns	12 224/2242	25 679/2600	25 801/2616
GooF	1.001	1.013	1.003
*R*1	0.0641	0.0361	0.0202
*wR*2	0.1231	0.0923	0.0389

[a] $R1 = \Sigma||F_o| - |F_c||/\Sigma|F_o|$, $wR2 = [\Sigma[w(F_o^2 - F_c^2)^2]/\Sigma[w(F_o^2)^2]]^{1/2}$, $w = 1/[\sigma^2(F_o^2) + (aP)^2 + bP]$, where $P = [\max(F_o^2,0) + 2F_c^2]/3$.

Table 2. Selected Bond Lengths (Å) and Angles (deg) for [M(II)(Bz$_2$pipdt)(mnt)] 1 (M = Ni), 2 (M = Pd), and 3 (M = Pt)[a]

Ni−S(1)	2.156(2)	S(1)−Ni−S(1)′	91.4(1)
Ni−S(2)	2.134(2)	S(2)−Ni−S(2)′	93.0(1)
C(1)−S(1)	1.690(6)	S(1)−Ni−S(2)	174.17(7)
C(10)−S(2)	1.716(7)	S(1)−Ni−S(2)′	88.13(7)
C(1)−C(1)′	1.48(1)	C(1)−S(1)−Ni	105.9(2)
C(10)−C(10)′	1.39(1)	C(10)−S(2)−Ni	103.7(2)
C(11)−N(2)	1.145(8)		
Pd−S(1)	2.2893(9)	S(1)−Pd−S(1)′	88.61(5)
Pd−S(2)	2.2747(9)	S(2)−Pd−S(2)′	90.35(5)
C(1)−S(1)	1.688(3)	S(1)−Pd−S(2)	176.24(4)
C(10)−S(2)	1.734(4)	S(1)−Pd−S(2)′	90.64(3)
C(1)−C(1)′	1.499(7)	C(1)−S(1)−Pd	105.4(1)
C(10)−C(10)′	1.354(7)	C(10)−S(2)−Pd	102.2(1)
C(11)−N(2)	1.136(5)		
Pt−S(1)	2.2780(9)	S(1)−Pt−S(1)′	88.19(5)
Pt−S(2)	2.2689(9)	S(2)−Pt−S(2)′	90.32(5)
C(1)−S(1)	1.691(3)	S(1)−Pt−S(2)	176.39(3)
C(10)−S(2)	1.735(3)	S(1)−Pt−S(2)′	90.85(4)
C(1)−C(1)′	1.490(6)	C(1)−S(1)−Pt	106.0(1)
C(10)−C(10)′	1.343(6)	C(10)−S(2)−Pt	102.1(1)
C(11)−N(2)	1.131(4)		

[a] The prime (′) = $-x$, y, $1/2 - z$.

donor systems of the two ligands are not exactly coplanar. The distortion is more pronounced for the Ni(II) complex (dihedral angle between the two donor sets planes of 8°) than the Pd(II) or Pt(II) complexes (dihedral angle of 5°). The benzyl residues of the Bz$_2$pipdt ligand in the three complexes are oriented in an up and down fashion conferring to the molecules a propeller-like shape. As reported in Table 2, the M−S bond distances involving the mnt ligand are slightly shorter than those originating from Bz$_2$pipdt whereas the C−S bond distances are longer as predicted according to the *push*−*pull* nature of the ligands. The sequence of M−S bond distances follows the ionic radii trend of the triad: Ni(II) < Pd(II) ≈ Pt(II).[13,7a,7b] The difference between C−C and the C−S distances in the C_2S_2 units of the $C_2S_2MS_2C_2$ core points out a different electronic distribution at the ligands and suggests a localized π-electron distribution in the complexes (structure A in Scheme 1), in accordance with a prevailing dithiolato character for mnt (*pull* ligand) and dithione one (*push* ligand) for Bz$_2$pipdt. Vibrational spectra of **1**, **2**, and **3** are in agreement with structural findings. Vibrations related to the common Bz$_2$pipdt group are found approximately at the same wavenumbers for the triad (the typical C−N vibrations of the thioamidic groups are observed as strong peaks in the IR at 1528 (Ni), 1531 (Pd), and 1528 (Pt) cm^{-1}, while the most significant peaks relatable to mnt show some differences between **1** and **2** and **3**. In particular, IR spectra exhibit peaks due to ν(CN) and ν(CC) stretching vibrations at 2187 and 1464 cm^{-1} (Ni), 2205 and 1495 cm^{-1} (Pd), and 2206 and 1487 cm^{-1} (Pt). In the Raman spectra the peaks relatable to CC stretching vibrations of mnt are found at 1472, 1496, and 1489 cm^{-1} for **1**, **2**, and **3**, respectively. Previous studies have shown that that the C═C stretch shifts to higher frequencies as the negative charge of the complex increases and is taken as a convenient marker for the oxidation level of a given coordinated dithiolene ligand.[14] By taking as reference the symmetric species $[M(mnt)_2]^{1-,\,2-}$ vibrational analyses show that this peak occurs near 1435 cm^{-1}in the monoanion and near

dx.doi.org/10.1021/ic2007765 |*Inorg. Chem.* 2011, 50, 10015–10027

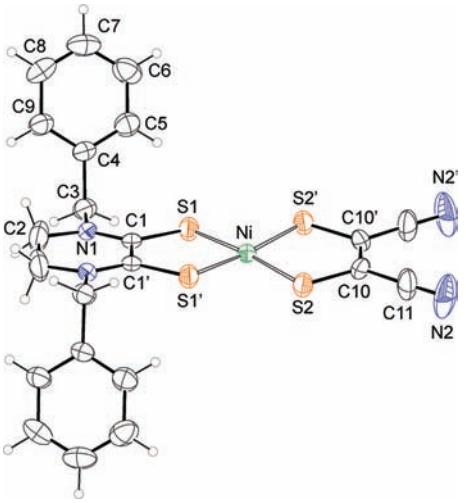

Figure 1. ORTEP drawing of [M(Bz$_2$pipdt)(mnt)] **1** (M = Ni) with the atom-numbering scheme adopted also for **2** (M = Pd) and **3** (M = Pt) with thermal ellipsoids at the 30% probability level. Symmetry code $' = -x, y, 1/2 - z$.

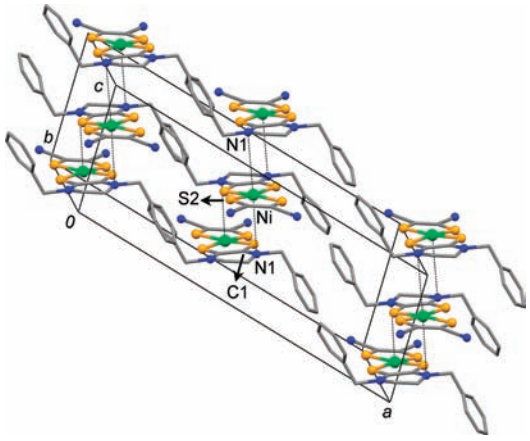

Figure 2. Crystal packing of [Ni(Bz$_2$pipdt)(mnt)] projected along the *b* axis. Hydrogen atoms were removed for clarity.

1485 cm^{-1} in the dianion, and this shift reflects the CC distance variation. The observed values in **1**−**3** further support that mnt behaves as a dithiolato bearing a formal charge close to 2−.

The crystal packing of [Ni(Bz$_2$pipdt)(mnt)] (Figure 2) shows that the molecules are stacked in an antiparallel arrangement, and these stacks are approximately aligned along the *c* axis. The Ni(II) atoms are interposed between two nitrogen atoms of symmetry related ligands (d[Ni−N(1)] = 3.741(6) Å), whereas the S(1) sulfur atom lies ∼3.74 Å above the C(1)−C(1) bond, Figure 2. Within the stacks, the N(2) nitrogen atoms of the mnt ligands are oriented toward the C(2) carbon atoms of the ethylene fragment of the Bz$_2$pipdt ligands, thus generating a layer that is parallel to the *bc* plane. The layers interact with each other by means of a partial π interaction between the aromatic rings of the Bz$_2$pipdt ligands. In fact, only the C(8) and C(9) carbon atoms are located at an interacting distance with symmetry related ones (∼3.68 Å), Figure 2. Despite the fact that **1** and **3** crystallize in two different space groups, the crystal packing of both compounds is very similar. In fact, **3** exhibits also layers formed by antiparallel molecules stacked along the *c* axis. The Pt(II) atom is located between symmetry related N(1) nitrogen atoms (d[Pt−N(1)] = 3.788(3) Å), Figure 3a. The major difference between the two crystal packings resides in the orientation of the benzyl moieties of **3** when compared to that of **1**. In fact, in **3**, adjacent layers have the aromatic rings that are roughly perpendicular to each other and show the C(6)−H group that points toward the centroid of a symmetry related aromatic ring (d[C(6)−Centroid] ∼ 3.91 Å, Figure 3b). In addition, within each layer, two antiparallel stacked complex molecules exchange two CH−π interactions[15] by means of the C(7) and C(9) carbon atoms (d[C(7)−C(9)] = 3.721(6) Å).

Complexes **1**, **2**, and **3** are characterized in the visible region by a broad absorption at 751 (660 sh), 651 (560 sh), and 685 nm in DMF with low to medium molar absorption coefficients [1.3 × 10^3 (**1**), 4.3 × 10^3 (**2**), and 10.1 × 10^3 (**3**) M^{-1} cm^{-1}] and a negative solvatochromism displayed in Figure 4 for **3** as an example. The energy of the solvatochromic peak shows a linear dependence on the solvent polarity parameter proposed by Cummings and Eisenberg for d^8-metal diimine−dithiolato complexes.[2b] The solvatochromic shifts determined as the gradient of this plot fall in the range found

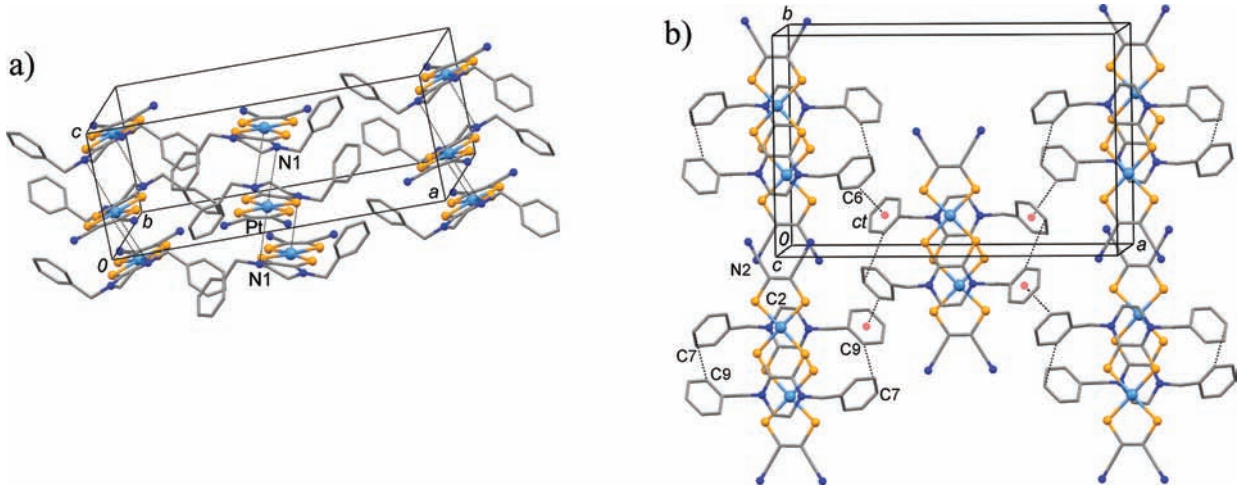

Figure 3. Crystal packing of [Pt(Bz$_2$pipdt)(mnt)] projected along the *b* axis (a, left side) and along the *c* axis (b, right side); ct = aromatic ring centroid. Hydrogen atoms were removed for clarity.

dx.doi.org/10.1021/ic2007765 |*Inorg. Chem.* 2011, 50, 10015–10027

Table 3. Summary of the Visible Absorption Spectra and Quadratic NLO Activity Data for the [M(Bz$_2$pipdt)(mnt)] Ni Triad

[M(Bz$_2$pipdt)(mnt)]	λ_{max}/nm	$\varepsilon \times 10^{-3}$/mol^{-1} dm^3 cm^{-1}	$\mu\beta_\lambda$[a]/10^{-48} esu[b]	$\mu\beta_0$/10^{-48} esu[b]
M = Ni(II), **1**	751 (660sh)	1.3	−1436	−463
M = Pd(II), **2**	651 (560sh)	4.3	−1450	−684
M = Pt(II), **3**	685	10.1	−1950	−822

[a] Measured at 1.907 μm using DMF solutions by electric-field-induced second-harminic generation (EFISH); uncertainty about 10%. [b] The conversion coefficient from esu units to MKS is 1.3972×10^{-21}, with the final value measured in C m^5 V^{-1}.

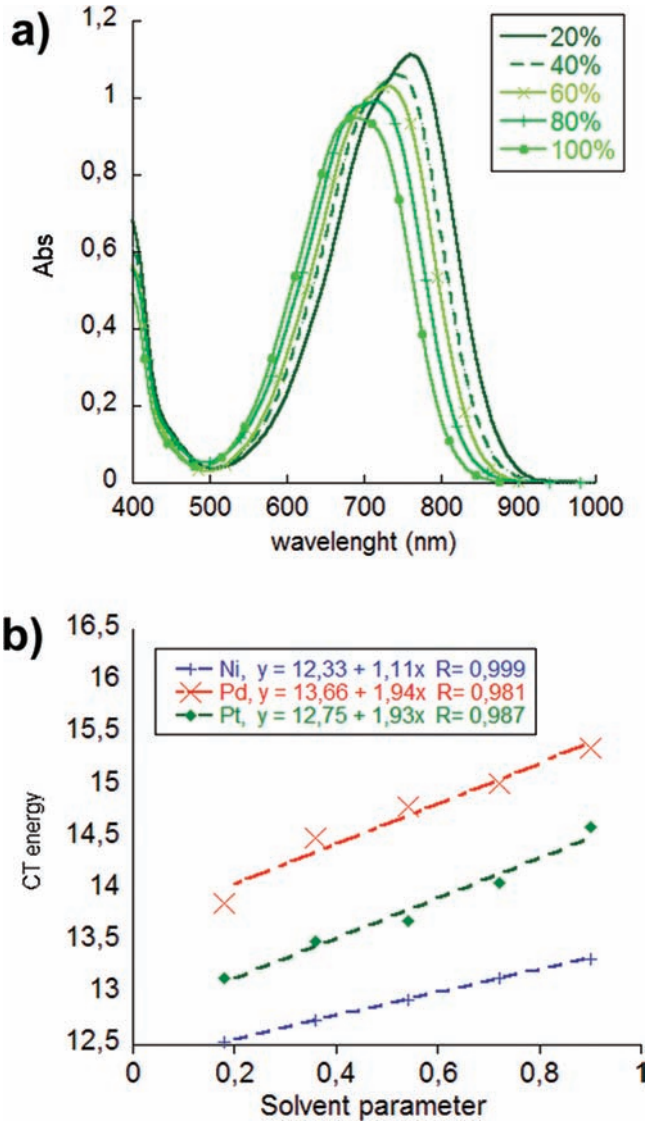

Figure 4. (a) Solvatochromic behavior of **3** in DMF/CS$_2$ mixtures ranging from DMF 100% to 20%. (b) Energy of the solvatochromic peak of **1**, **2**, and **3** versus the solvent polarity parameter for solutions in DMF/CS$_2$ mixtures ranging from DMF 100% to 20%.

for d^8-metal diimine−dithiolato complexes, and the values for the Pt and Pd derivatives are higher than the one obtained in the Ni case.

The molecular quadratic optical nonlinearities were determined by the EFISH (electric-field-induced second-harmonic generation) technique. The set up used allows determination of the scalar product $\mu\beta_\lambda$ (μ = ground-state dipole moment; β_λ = projection of the vectorial component of the quadratic hyperpolarizability tensor along the dipole moment axis).[16] Measurements performed at 1907 nm and using DMF solutions provide $\mu\beta_\lambda$ values with an uncertainty of about 10%. These and the $\mu\beta_0$-extrapolated values to zero frequency (where β_0 is the static quadratic hyperpolarizability) have been calculated applying eq 1

$$\mu\beta_0 = \mu\beta_\lambda[1 - (2\lambda_{max}/\lambda)^2][1 - (\lambda_{max}/\lambda)^2] \quad (1)$$

where $\mu\beta_\lambda$ values are determined at incident wavelength λ =1907 nm and λ_{max} is the absorption wavelength of the charge-transfer transition considered.

These data, collected in Table 3, show that these complexes exhibit large negative second-order polarizabilities, larger than those so far reported for d^8 metal diimine−dithiolato complexes, where a maximum value of $\mu\beta_0 = 480 \times 10^{-48}$ esu in DMSO was obtained for a platinum derivative.[6]

In this case also, it can be noted that the platinum complex exhibits the largest molar absorptivity as well as second-order polarizability in the metal triad. NLO activity is also expected for **1**, **2**, and **3** when embedded in poled polymers but not when they formed pure crystals, since they crystallize in a centrosymmetric space group.

Cyclic voltammetric experiments performed on DMF solutions of the complexes show that **1**, **2**, and **3** are redox active and exhibit two reversible reduction waves and one irreversible oxidation wave, see CV scans of **2** in Figure 5 as an example, at potentials reported in Table 4 and Figures S1−S4, Supporting Information, showing the linear dependence of the peak currents (ip) from the square root of the voltage scan rate in the case of complex **2** (ip_{red}/ip_{ox} is close to the unity). The reduction values are close to those found for other mixed-ligand complexes bearing the R$_2$pipdt ligand.[7d,11] In Table 4, data for [Ni(M$_2$pipdt)(mnt)] are reported to show the influence of Bz vs Me substituents by making easier the reduction of the complex. We suggest that the reduction processes predominantly involve Bz$_2$pipdt, in agreement with its predictable predominant contribution to the LUMO, and that the

Table 4. Cyclic Voltammetric Data[a]

[M(Bz$_2$pipdt)(mnt)]	E_a (V)[b] 0 → 1+	$E^1_{1/2}$ (V)[c] 0 ⇆ 1−	$E^2_{1/2}$ (V)[c] 1− ⇆ 2−
M= Ni(II), 1	+1.09	−0.39	−0.90
M= Pd(II), 2	+1.20	−0.35	−0.84
M= Pt(II), 3	+1.08	−0.37	−0.87
[Ni(Me$_2$pipdt)(mnt)][d]	+0.91	−0.53	−0.96

[a] Measured at a Pt electrode in DMF, 0.1 M Bu_4NPF_6, scan rate 100 mV/s, and reference electrode Ag/AgCl. [b] Irreversible anodic broad wave. [c] Reversible reduction waves. One additional reduction wave appears at −1.29 V for the Ni derivative. [d] Reported for comparison reasons, see ref 7b.

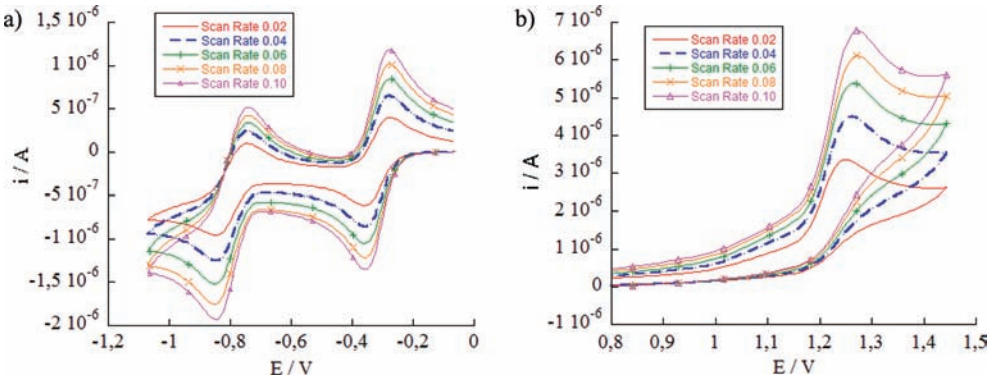

Figure 5. Cyclic voltammograms of **2**, as an example, in argon-degassed DMF solutions containing 0.1 mol dm^{-3} Bu_4NPF_6, measuring the current (I) response to a cycled potential (E): (a) **2** shows two reduction reversible processes; (b) the complex also undergoes one irreversible oxidation process at positive potential. Cyclic voltammetric data for **1**, **2**, and **3** are collected in Table 4.

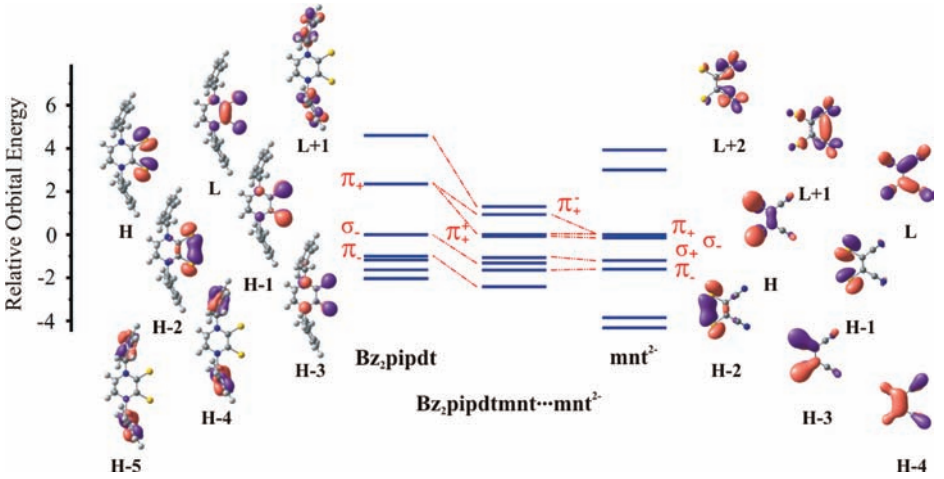

Figure 6. Molecular orbital diagram of the two ligands along with their hypothetical interaction scheme.

oxidation process should involve mnt due to its expected contribution to the HOMO. With regard to the irreversibility of the oxidation peak, the reason for this irreversibility is not clear. The appearance of an insoluble precipitate as a consequence of the oxidation may suggest that the oxidized species is insoluble or undergoes decomposition.

Calculated Molecular Structures. The optimized structures of **1**−**3** together with the calculated data are given in the Supporting Information (Figure S5 and Table S1, respectively). The DFT-optimized bond lengths and angles of **1**, **2**, and **3** well describe the experimental structures; bond lengths are reproduced within 0.03 Å. Moreover, calculated data further support that **1**−**3** belong to the *push*−*pull* type of complexes and that their electronic properties are relative to [M(diimine)(dithiolato)] complexes.[2−6,17,18]

In general, the M−S bond lengths increase in the order Ni−S < Pt−S ≈ Pd−S. On one hand, this is due to the smallest bonding radius of Ni and on the other to the relativistic effects, which govern the third-row metals and contract several inner atomic orbitals. This series also agrees with the ionic radii of the d^8 metals (78 pm for Pd(II) and 74 pm for Pt(II)). It must be underlined that in order to well reproduce this series a combination of Dirac−Fock relativistic-type pseudopotentials and valence triple-ζ quality basis sets has to be applied to all atoms. Moreover, M−S distances in the case of the dithiolato ligand seem to be shorter than the relative distances in the dithione, indicating a difference in bonding between the *push* and the *pull* ligand. For the chelated five-membered dithiolene rings, the C−C and C−S bonds should be indicators of the electronic properties that are induced through complexation. For the *push* 1,2-dithione the C−C bond is expected to be longer than the relative bond in an electron-accepting *pull* 1,2-dithiolate, whereas this is opposite for the C═S bond. Indeed, this is what is observed; the C−C bond distance is ∼1.36 Å in mnt ligand but ∼1.49 Å in Bz_2pipdt (1.40 Å in benzene), while C−S is ∼1.73 Å in mnt and ∼1.69 Å in the piperazine ligand (S−C(sp^2) ≈ 1.751 Å).

Electronic Structure and Role of Solvent. In order to assign the absorption bands and in particular to determine the metal and ligand contributions to the highest and lowest occupied MOs as well as the solvent effect, DFT calculations[19] in vacuum and in two polar solvents, namely, acetonitrile and dimethylsulfoxide, were performed on all three complexes according to the computational section. Computational details with related references are reported in the Experimental Section. The two polar solvents were selected in order to reproduce the experimental results since our complexes were soluble in them. On the other hand, we have already shown that the behavior of a relevant type of

Table 5. Contribution of Different Fragments to Complexes Valence Orbitals[a]

MO	*E*, eV	Bz_2pipdt	M	mnt
		1		
		unoccupied		
68a	−1.66	8.9	2.1	89.0
65b	−2.51	23.0	44.2	32.7
64b	**−3.96**	**79.7**	**4.8**	**15.6**
		occupied		
63b	**−5.54**	**20.0**	**10.0**	**70.0**
67a	−6.66	7.9	34.2	57.9
66a	−7.05	9.9	75.8	14.3
		2		
		unoccupied		
68a	−1.59	0.9	1.4	97.7
65b	−2.48	26.7	34.4	38.9
64b	**−3.94**	**80.4**	**4.7**	**14.8**
		occupied		
63b	−5.48	19.3	8.2	72.5
67a	−6.64	10.7	26.2	63.1
66a	−7.14	3.1	75.9	21.0
		3		
		unoccupied		
68a	−1.69	0.2	1.5	98.3
65b	−1.86	31.5	32.3	36.2
64b	**−3.89**	**75.2**	**7.5**	**17.3**
		occupied		
63b	**−5.56**	**26.1**	**10.4**	**63.5**
67a	−6.49	19.1	33.9	46.9
66a	−7.26	18.4	63.6	18.0

[a] HOMO and LUMO orbitals are shown in bold.

compounds upon solvation to nonpolar solvents is analogous to that in the gas phase and that the nature of the solvent is crucial when one wants to reveal the metal contribution to the electronic structure of the complexes.[17e]

Before going on in our discussion of the properties of the complexes, it is instructive to study the electronic structure of the ligands that coordinate the metal. Thus, in Figure 6 contour plots of the frontier orbitals of both ligands under study, the dithione Bz_2pipdt and the dithiolato mnt^{2-}, are presented. For the sake of clarity, the chelating moieties S−C−C−S are considered almost planar; then the resulting MOs can be divided into two categories: the out-of-plane (π) and the in-plane (σ) orbitals. In addition, the orbitals are subdivided into in phase (+) and out of phase (−) in each category. The two π_+ orbitals are very important in the bonding scheme since they are bonding with respect to the C−C bond but antibonding to the C−S bonds. Thus, upon population they result in shrinkage of C−C bonds but in elongation of C−S. In order to reveal their contribution, a working hypothesis with the two ligands Bz_2pipdt and mnt^{2-} being at the same energy level that occupy in **3** but without the central metal is taking in account. For this ligand cage, the aforementioned out-of-plane orbitals form positive (π_+^+) and negative (π_+^-) combinations, but it is only the latter that owns the correct symmetry in order to interact with a metal d orbital, d_{xz} in our case. The strength of the interaction depends on the relative orbital energies and overlap. In the ligand cage encountered there are of course both attractive and repulsive S···S interactions with the latter playing an important role as mentioned before. This is the formation of $\pi_+^+$and π_+^-, which are formed by the interaction of the Bz_2pipdt LUMO with the mnt HOMO, both being higher in energy than the metal d_{xz} orbital (Figure 6). As a result, ligand orbitals are significantly destabilized compared to the metal's d parentage. This generates an *inverted bonding scheme* in consequence with what has been adopted for other dithiolate complexes, whereas in a normal bonding scheme the metal *n*d orbitals lie at higher energies compared to the ligand orbitals.[20,21]

Turning to the properties of the complexes, Table 5 shows the contribution of different fragments (the two ligands and the central metal) to the complexes' frontier orbitals in the gas phase, while in Figure 7 an energy level diagram of **1**−**3** is provided along with contour plots of the frontier orbitals of **2**. This is necessary in order to compare our results with previous ones in the literature, where all calculations were performed under vacuum.[7b] As our complex belongs to the C_2 point group, the HOMO is π_+ antibonding with respect to the M−S (mnt) bonds whereas the LUMO is a π_- combination of the d_{xz} metal orbital and the unoccupied Bz_2pipdt π_+ orbital mentioned above. The existence of these interactions, along with the significant contributions of 1,4-dibenzylpiperazine-2,3-dithione's orbital to the HOMO (20.0%, 19.3%, and 26.1% for **1**, **2**, and **3**, respectively) and maleonitriledithiolato orbital contributions to the LUMO (15.6%, 14.8%, and 17.3% for **1**, **2**, and **3**, respectively) is consistent with π^*-backdonation theory.[17e,5a]

Backdonation from the metal/π^*-dithiolato moiety toward the dithione ligand is evident in both the HOMO and the LUMO orbitals. In the three complexes under study, the HOMO is raised mainly by a charge donation from M/mnt's high occupied frontier orbital (HOFO) to dithione's lower unoccupied frontier orbital (LUFO), while the LUMO is constructed mainly by the latter, which accepts electron density from M/mnt's HOFO, along with a small contribution from HOFO-3, an orbital of the same local symmetry. The whole bonding scheme in the case of **3** is depicted in Figure 8.

From the four remaining lowest unoccupied orbitals, LUMO +3 and LUMO+4 are mainly dithione based π^* orbitals. On the other hand, 65*b*, a strongly σ-antibonding one, carries "in-plane" interactions formed from the four sulfur atoms and the central metal, whereas LUMO+2, is a mnt-based orbital of a local a_2 symmetry. The existence of a relatively low-lying orbital localized on the *push* ligand is reported to be involved in a dithiolato-based emitting state in the [Pt(diimine)(dithiolato)] complexes. The observation of no luminescence in compound **3**,[22] although it is due to the fast excited-state deactivation, could be also attributed to an extensive mixture of the ligands orbitals.[5,23] HOMO-1 is mainly M−mnt in nature and is raised by antibonding interactions between an a_2 ligand orbital (under local symmetry) and the d_{yz} orbital of the metal. HOMO-3 (for **1** and **3** but HOMO-5 for **2**) and HOMO-4 are also π orbitals. Both contain mainly antisymmetric interactions of ligand orbitals to metal's d_{xz} and d_{xy} orbitals. Finally, HOMO-2 and HOMO-5 (HOMO-3 for **2**) contain bonding metal−ligand contributions with the former being mainly a metal-centered orbital ($d_{x^2-y^2}$). Of course, molecular distortion upon HOMO depopulation plus interaction with the solvent can be another excited-state deactivating factor.

dx.doi.org/10.1021/ic2007765 |*Inorg. Chem.* 2011, 50, 10015–10027

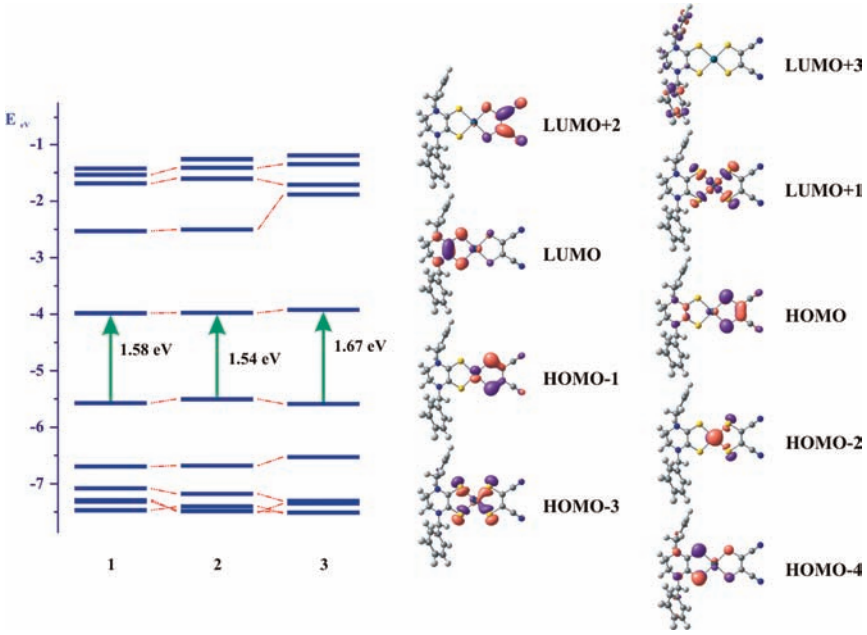

Figure 7. Energy level diagram of **1**−**3** along with 0.05 au contour plots of the frontier orbitals of **2**.

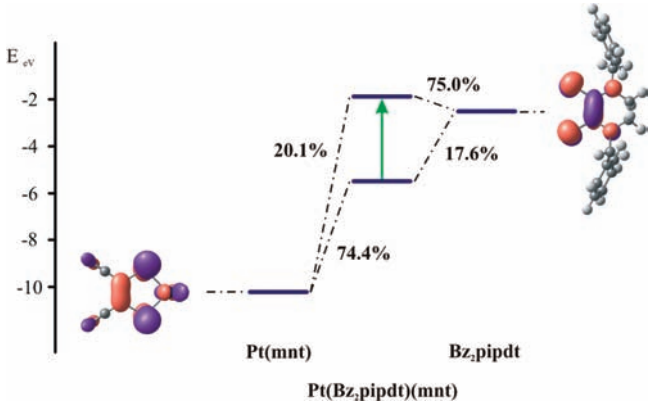

Figure 8. Fragment molecular orbital analysis for **3**.

The influence of the *solvent*−*solute* interactions on the electronic properties of complexes **1**−**3** is indicated by employing the polarizable conductor calculation model (CPCM) for acetonitrile and dimethylsulfoxide. These interactions yield an increase of the HOMO−LUMO gap and of the HOMO and LUMO localization. In Table 6 and Table S3, Supporting Information, the contribution of different fragments (the two ligands and the central metal to the complexes' frontier orbitals in the presence of a DMSO electric field is reported. These data show that the relative energy order becomes Pd > Pt ≈ Ni, in accordance with our experimental data and different from the observed trend in the gas phase: Pt > Ni > Pd. This result further supports our previous findings about the role of the solvent when complexes with identical ligands but different metal are studied.[17e] The role of the metal is crucial for delocalization of the frontier orbitals. According to a simplified two-state model,[16] a lower degree of delocalization of frontier orbitals, as is the case for the palladium complex, results in a larger difference between the excited-state and the ground-state dipole moment ($\Delta\mu_{ge}$);[17e] this leads to an increase of the negative solavatochromism of this type of compounds. This outcome is verified by our experiments, with the palladium and platinum being significantly solvatochromic (see the solvatochromic shifts in Figure 4).

In other words, the palladium compound with the largest charge separation in the ground state (∼0.7 vs ∼0.6 e^- for Pt and Ni) is affected the most by the solvent field, as expected (vide supra). Data in Table 6 reveal that the occupied orbitals are stabilized by the field of the solvent, whereas the unoccupied ones are destabilized compared with the gas phase (Table 5). Changes in the order of the orbital's energy from the gas phase (and in nonpolar solvents, if soluble) to the DMSO field are pictorially depicted in Figure 9. These changes are expected to have an impact in the visible spectra side features of these complexes, expressed mainly through changes in the character of the transitions that lie higher in energy.

Moreover, solvation seems to have a further impact on the character of the frontier orbital. Comparison of the data in Tables 5 and 6 indicates that upon including the solvent the HOMO and LUMO become more localized on the M(mnt) fragment (∼10%) and Bz_2pipdt ligand (∼13%), respectively. In other words, frontier orbitals in all compounds under study become more localized in polar solvents and as a result an enhancement in the properties that are related to the main charge-transfer band should be expected. On the other hand, backdonation seems to suffer a reduction due to the decreasing participation of Bz_2pipdt in the HOMO. In fact, this reduction is over ∼70%, e.g., in the case of **2**, and backdonation is reduced from a value of ∼14% (vide supra) to 2.5% in DMSO. The backbonding reduction in increasing the solvent's field may be of importance for proper selection of a solvent for a ligand-based reaction upon these complexes.

Our results support also the redox data reported in Table 4. The HOMO of **2** is the most stabilized along the relative series, and this fact is illustrated by its more positive E_{ox}. On the other hand, the almost identical piperazine contribution to the LUMOs would lead to almost equal first reduction potentials for the three complexes, in accordance with our experimental results.

dx.doi.org/10.1021/ic2007765 |*Inorg. Chem.* 2011, 50, 10015–10027

Table 6. Contribution of Different Fragments to Complexes Valence Orbitals in the Presence of a DMSO Electric Field[a]

MO	*E*, eV	Bz_2pipdt	M	mnt
		1		
		unoccupied		
65b	−2.15	20.2	54.2	25.6
68a	−2.24	0.6	1.3	98.1
64b	**−3.51**	**93.0**	**3.5**	**3.4**
		occupied		
63b	**−5.70**	**15.0**	**19.8**	**65.2**
67a	−6.43	20.8	61.5	17.7
66a	−6.48	9.1	93.5	−2.6
		2		
		unoccupied		
68a	−2.20	0.1	1.3	98.6
65b	−2.58	29.0	35.2	35.8
64b	**−3.47**	**93.8**	**2.8**	**3.5**
		occupied		
63b	**−5.72**	**9.7**	**12.3**	**78.0**
67a	−6.71	37.1	31.6	31.3
66a	−7.01	87.4	11.4	1.2
		3		
		unoccupied		
65b	−1.90	29.7	33.6	36.7
68a	−2.23	0.1	1.6	98.3
64b	**−3.47**	**91.1**	**4.0**	**4.9**
		occupied		
63b	**−5.67**	**16.2**	**17.1**	**66.7**
67a	−6.48	34.9	36.6	28.6
66a	−7.02	96.5	2.7	0.8

[a] HOMO and LUMO orbitals are shown in bold.

Absorption Spectroscopy. TD-DFT calculations well interpret the experimental spectral features of all three complexes (Tables S4, S5, and S6, Supporting Information). In Table 7 the TD-DFT-calculated energies and compositions of the lowest lying singlet electronic transitions responsible for the main absorption band in the visible region of **1**, **2**, and **3**, shown in Figure 10, are reported. In these tables we use the following abbreviations: MMLL′CT = mixed-metal−ligand-to-ligand charge transfer, MLCT = metal-to-ligand charge transfer, LMCT = ligand-to-metal charge transfer, LL′CT = ligand-to-ligand charge transfer, and IL = intraligand charge transfer. The transitions under study fulfill the criteria posed by Casida.[24]

The main feature of the low-energy region of the UV−vis spectra of the complexes under study is the existence of a highly negative solvatochromic band. This band is accompanied by a second one, which appears either as a shoulder in the high-energy edge or just widens the main band. The former is raised by the transition $a^1A \rightarrow b^1A$ and can be described as a mixed-metal−ligand-to-ligand charge-transfer band (MMLL′CT). This type of transition is observed also in the related *push−pull* complexes [M(diimine)(dithiolato)][17e,f,5a,2b,2c] and is linked to their enhanced nonlinear optical properties, such as the relatively high values of molecular hyperpolarizability.[2c] The transition can be up to a point described as a HOMO → LUMO one. On the other hand, the populated state has a slight multiconfigurational character, since the contribution of the latter is predominant (∼83% in **2** and **3**) but not unique.

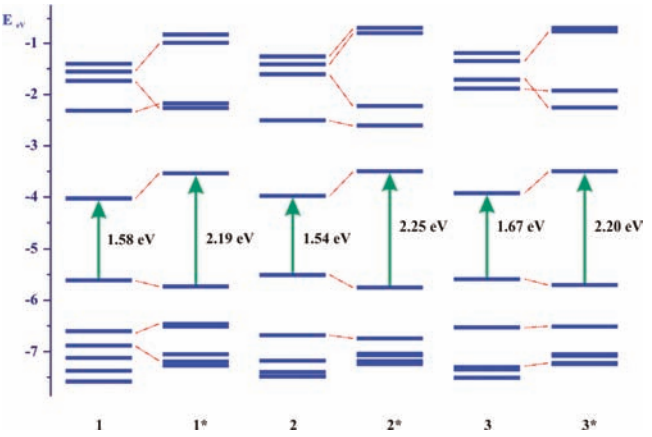

Figure 9. Energy level diagram that depicts the relation between the orbitals calculated in the gas phase with the ones calculated within the CPCM approximation employing DMSO as the solvent. The latter are denoted with the asterisk.

Complex **2** exhibits a shoulder in the high-energy side of the main band. This feature can be characterized as a mixed LMCT/LL′CT HOMO → LUMO+1 transition, and it is noticeable that it is not observed in **3** due to the very low value of the oscillator strength of the relative $a^1A \rightarrow c^1A$ transition.

A different behavior is observed in the case of the nickel compound. Both the main band and the observed shoulder, having a multiconfigurational character, can be characterized as MMLL′CT HOMO → LUMO and LMCT HOMO → LUMO+2 transitions and well reproduce the experimental feature (Figure 10).

These calculations compared to the ones in the gas phase reveal the importance of the solvent, within the CPCM approximation, in the case of the first-row metal complex **1**. Thus, although gas-phase calculations lead to the same interpretation of the main band in all three complexes, TD-DFT calculations within the CPCM approximation with polar solvents reveal the role of the metal upon solvation, fully supporting the experimental finding (Table 6 and Figure 10). Finally, shifts of the lowest lying allowed transitions to shorter wavelengths and the intensity variations are well reproduced by calculations for all three complexes and can be characterized as MLCT, LMCT, and ILCT types (Table S4−S6, Supporting Information).

Molecular Hyperpolarizabilities. In an effort to elucidate the second-order response of compounds **1**−**3** and to complement our EFISH results, we employed the computation of the static and dynamic hyperpolarizabilities according to the coupled perturbed Hartree−Fock methodology (references quoted in Experimental Section, Computational Details). Within this framework and trying to reproduce experimental conditions as accurately as possible, we employed the polarizable conductor calculation model (CPCM) in order to simulate DMSO's electric field. DMSO is a very polar solvent and has proved to induce analogous solvation interactions to DMF, which was the solvent used in our EFISH experiments; actually λ_{max} = 736 (ε = 1700), 634 (4950), and 672 (8250) for Ni, Pd, and Pt, respectively, in

dx.doi.org/10.1021/ic2007765 |*Inorg. Chem.* 2011, 50, 10015–10027

Table 7. TD-DFT-Calculated Energies and Compositions of the Lowest Lying Singlet Electronic Transitions Responsible for the Main Absorption Band in the Visible Region of 1, 2, and 3

state	composition[a]	ΔE[b]	exp.[c]	f[d]	character
b^1A	HOMO → LUMO, 44%	1.65	1.65	0.1153	mnt/Ni/Bz_2pipdt → Bz_2pipdt (MMLL′CT)
	HOMO → LUMO+2, 31%				mnt/Ni/Bz_2pipdt → Ni/mnt/Bz_2pipdt (LMCT)
	HOMO-3 → LUMO+2, 9%				Ni/Bz_2pipdt/mnt → Ni/mnt/Bz_2pipdt (LMCT/*deloc.*)
b^1A	HOMO → LUMO, 84%	1.81	1.90	0.1532	mnt/Pd/Bz_2pipdt → Bz_2pipdt (MMLL′CT)
a^1B	HOMO → LUMO+1, 89%	2.11	2.21sh	0.0166	mnt/Pd/Bz_2pipdt → mnt/Pd/Bz_2pipdt (LMCT/LLCT)
b^1A	HOMO → LUMO, 82%	1.84	1.81	0.2638	mnt/Pt/Bz_2pipdt → Bz_2pipdt (MMLL′CT)

[a] Compositions of electronic transitions are expressed in terms of contributing excitations between ground-state Kohn−Sham molecular orbitals. The calculation provided was done employing a 10MDF core potential for the nickel, since the latter shows a slightly better behavior as compared to data extracted with 10MHF. Difference was ~0.1 eV. [b] Transition energy from the a^1A ground state in eV. [c] Values for a DMF solution. [d] Oscillator strength.

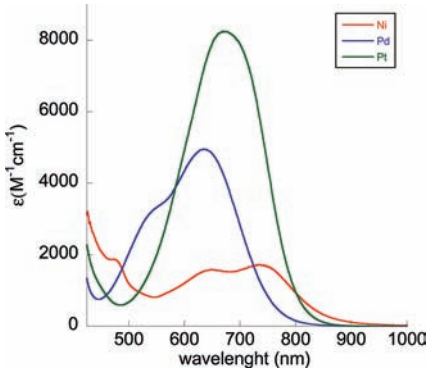

Figure 10. Absorptivities of **1**, **2**, and **3** in DMSO solutions ($c \times 10^{-4}$ mol dm^{-3}, 1.0 cm silica cell).

Table 8. Calculated Hyperpolarizability β_{vec} Values for 1−3 (in 10^{-30} esu)

complex	static/10^{-30} esu	$\hbar\omega$ = 0.65 eV/10^{-30} esu	$\mu\beta^a/10^{-48}$ esu
1	−1.7	−1.8	−74
2	−3.6	−3.1	−124
3	−12.0	−12.0	−489

[a] μ (calculated by CPHF and CMCM) is equal to 41, 40, and 41 D for **1**, **2**, and **3** respectively; 1D = 10^{-18} esu.

DMSO. In addition, we selected 0.65 eV (1904 nm) to be our theoretical laser fundamental radiation, which was also employed during the experimental procedure.

The first hyperpolarizability of **1**−**3** was calculated according to the following equations, and the results for both static and dynamic β are provided in Table 8.

$$\beta_i = \beta_{iii} + \frac{1}{3}\sum_{1\neq k}(\beta_{ikk} + \beta_{kik} + \beta_{kki}), \text{with } i,k = x,y,z \quad (2)$$

$$\beta_{vec} = \sum_i \frac{\mu_i \beta_i}{\mu_g} \quad (3)$$

According to our results, all three compounds show second-order response. While the calculated values, when compared with experimental data obtained by EFISH measurements, seem to be underestimated, the experimentally observed trend of the metal is fully supported. In particular, the platinum complex shows the largest beta values of the series followed by palladium and nickel ones.

This conclusion is in agreement with our experimental results and is also qualitatively supported by results published on relative compounds.[25] Although the organic molecules that are already employed for applications show better responses than our complexes, it is likely that *push*−*pull* dithiolenes of a proper structure could possibly replace organic molecules in the future.[26]

CONCLUSIONS AND PERSPECTIVES

Synthesis, structural, spectroscopic, and electrochemical studies, second-order NLO measurements, and theoretical calculations have been performed on the Ni triad of uncharged bis-dithiolene mixed-ligand complexes: [M(II)(Bz_2pipdt)(mnt)] (Bz_2pipdt = 1,4-dibenzyl-piperazine-3,2-dithione, mnt = maleonitriledithiolato, M(II) (Ni, **1**; Pd, **2**; Pt, **3**). DFT and TD-DFT calculations fully elucidated the electronic structure of these complexes, indicating the role of the metal and ligands, whereas employment of the CPCM model reveals the role of the solvent, indicating that a polar solvent stabilizes the localized orbitals on the dithiolato ligand whereas it destabilizes the orbitals on the dithione one. This result fully supports the experimental UV−vis and electrochemical data of the complexes under study. Additionally, the coupled perturbed Hartree−Fock methodology has been adopted to interpret the electronic origin of the NLO properties. The analysis accounts for the various NLO responses in terms of the more important components, showing that the most appealing candidate as a second-order NLO chromophore is the platinum compound. This is relatable to (i) the most extensive mixture of the dithione/metal/dithiolato orbitals in the case of the platinum compound vs nickel and palladium ones (a smaller energy gap for the charge-transfer transition should result in a larger β_0 value), (ii) the influence of the electric field of the solvent on the frontier orbitals that maximizes the difference in dipole moments between the excited and the ground state in the case of the platinum compound, and (iii) the largest oscillator strength of the platinum compound (0.2638 vs 0.1153 and 0.1532 for Ni and Pd compounds, respectively).

A systematic investigation varying the *push* and *pull* ligands is underway to probe the structure−property relationship and test the effect of the redox activity on the NLO properties of these

complexes, in particular to check their potential for applications in redox switching of molecular first hyperpolarizabilities.

EXPERIMENTAL SECTION

Chemicals. $NiCl_2 \cdot 6H_2O$, $[Pd(CH_3CN)_2Cl_2]$, and K_2PtCl_4, reagent-grade CH_3CN, Et_2O, and MeOH, and spectroscopic-grade DMF, CH_3CN, and DMSO were used as received from Aldrich.

Preparations. *[M(Bz$_2$pipdt)Cl$_2$].* $[Ni(Bz_2pipdt)Cl_2]$ was prepared in almost quantitative yield by reacting $NiCl_2 \cdot 6H_2O$ (MeOH solution) with a $CHCl_3$ solution of Bz_2pipdt[27] in equimolar ratios under reflux for 1 day. In the Pd and Pt cases more reactive starting reagents with respect to dichlorides have been used to improve the reaction yields. In fact, by using $[Pd(CH_3CN)_2Cl_2]$, commercially available, or $[Pt(DMSO)_2Cl_2]$, prepared according to ref 12, the desired products are obtained as shown in Scheme 2 in almost quantitative yields.

To prepare $[M(Bz_2pipdt)(mnt)]$ (M = Ni, **1**; M = Pd, **2**; M = Pt, **3**), a yellow MeOH solution of K_2mnt (easily obtained following the same well-known procedure used to prepare Na_2mnt[28]) (33.72 mg, 0.14 mmol in 25 mL) was added dropwise to a blue MeOH solution of $[Ni(Bz_2pipdt)Cl_2]$ (62.40 mg, 0.14 mmol in 25 mL) under stirring. The solution became dark-green and was allowed to react under reflux for 24 h. A dark-green solid was formed, filtered, washed with diethyl ether, and dried, obtaining 61.81 mg (94% yield). The obtained solid consisted of well-formed crystals, which can be also obtained through recrystallization from CH_3CN/Et_2O. Analytical results are in accordance with the formula $[Ni(Bz_2pipdt)(mnt)]$. Anal. Calcd for $C_{22}H_{18}N_4NiS_4$; C, 50.30; H, 3.45; N, 10.66; S, 24.41. Found: C, 50.3; H, 3.6; N, 10.5; S, 22.8. IR [KBr, cm^{-1}]: 2928vw, 2206vs, 2187vw, 1635m, 1528vs, 1497vw, 1464w, 1454w, 1437m, 1357m, 1263w, 1184m, 1149w, 1109w, 1081w, 862vw, 738m, 698m, 605vw, 574w, 548w, 511w, 471w. Raman (cm^{-1}): 2192s, 1538w, 1472vs, 1305m, 1295w, 1296m, 1191s, 1120s, 511m, 346m, 337m.

[Pd(Bz$_2$pipdt)(mnt)] (**2**). As described for **1**, **2** has been similarly obtained by reacting K_2mnt (31.80 mg, 0.13 mmol in 25 mL of MeOH) with $[Pd(Bz_2pipdt)Cl_2]$ (66.10 mg 0.13 mmol in 25 mL of DMF solution), obtaining 72.40 mg of a blue precipitate (yield 96%). The crude product was filtered, washed with Et_2O, and recrystallized from CH_3CN/Et_2O, following dissolution in CH_3CN with a Soxhlet extractor. Analytical results are in accordance with the formula $[Pd(Bz_2pipdt)(mnt)]$. Anal. Calcd for $C_{22}H_{18}N_4PdS_4$; C, 46.11; H, 3.17; N, 9.78; S, 22.38. Found: C, 45.5; H, 3.1; N, 9.5; S, 21.4. IR [KBr, cm^{-1}]: 2990vw, 2218vw, 2205vs, 1621m, 1531vs, 1495vw, 1454w, 1431m, 1367m, 1356m, 1253w, 1188m, 1147w, 1107w, 1087m, 860vw, 744m, 700m, 605vw, 574w, 549w, 507w, 468w. Raman spectra (cm^{-1}): 2347vw, 2209w, 1940vw, 1524s, 1496vs, 1436vw, 1322w, 1275m, 1191m, 1115w, 1105w, 528m, 353s, 149m.

[Pt(Bz$_2$pipdt)(mnt)] (**3**). A 62.03 mg amount (0.10 mmol) of $[Pt(Bz_2pipdt)Cl_2]$ in 25 mL of DMF and 25.80 mg (0.10 mmol) of K_2mnt in 25 mL of MeOH were reacted. A green-blue precipitate (56.13 mg) formation was observed immediately. The precipitate was filtered, washed with Et_2O, and recrystallized from CH_3CN/Et_2O. Yield: 94%. Analytical results are in accordance with the formula $[Pt(Bz_2pipdt)(mnt)]$. Anal. Calcd for $C_{22}H_{18}N_4PtS_4$; C, 39.93; H, 2.74; N, 8.47; S, 19.38. Found: C, 39.7; H, 2.6; N, 8.3; S, 19.2. IR [KBr, cm^{-1}]: 2918vw, 2224vs, 2206vw, 1527vs, 1487vw, 1454w, 1431m, 1373m, 1362 m, 1252ww, 1187m, 1156m, 1105w, 1087w, 864vw, 744m, 700m, 603vw, 574w, 551w, 502w, 467w. Raman spectra (cm^{-1}) 2209vw, 1521m, 1489vs, 143w, 1318m, 1303w, 1293vw, 1275m, 1192s, 1120m, 1047w, 1005w, 972w, 529 m, 405w, 374 m, 154w.

Microanalyses were performed by means of a Carlo Erba CHNS Elemental Analyzer model EA1108.

Spectroscopic Measurements. IR spectra (4000−350 cm^{-1}) were recorded on a Bruker IFS55 FT-IR Spectrometer as KBr pellets. Raman spectra were carried out at room temperature on single crystals using a LABRAM-Jobin Yvon spectrometer equipped with an integrated microscope (BX 40, Olimpus) for micro Raman measurements. The excitation wavelength has been a He−Ne (632.8 nm, 20 mW) laser, the laser power being reduced by a factor of 100 in order to avoid sample damage and degradation. A 100× objective has been used for injection of the laser line and collection of the Raman signal in the back-scattering configuration. The laser line is removed by an holographic super notch filter, and the Raman signal is dispersed by a stigmatic 300 mm focal length spectrometer equipped with two exchangeable gratings. A 1800 g/mm grating has been used to obtain the maximum in terms of spectral resolution (2.5 cm^{-1}). The signal is finally detected with CCD 1024 × 256 pixels cooled by a TE Peltier. The scattering peaks were calibrated against a Si standard (ν = 520 cm^{-1}). The typical spectrum was collected with a 500 s time constant and averaged over 5 scans. No sample decomposition was observed during the experiments.

Electronic spectra were recorded with a Cary 5 spectrophotometer. Cyclic voltammograms were carried out on a EG&G (Princeton Applied Research) potentiostat-galvanostat model 273 using a conventional three-electrode cell consisting of a platinum wire working electrode, a platinum wire as counter-electrode, and Ag/AgCl in saturated KCl solution as the reference electrode. Experiments were performed at room temperature (25 °C) in dry and argon-degassed DMF containing 0.1 mol dm^{-3} Bu_4NPF_6 as supporting electrolyte at a 20−100 mV s^{-1} scan rate. The half-wave potential for the ferrocene/ferrocenium couple (internal standard) is 0.43 V under the above conditions.

Data Collection and Structure Determination. A summary of data collection and structure refinement for $[Ni(Bz_2pipdt)(mnt)]$, $[Pd(Bz_2pipdt)(mnt)]$, and $[Pt(Bz_2pipdt)(mnt)]$ is reported in Table 1. Single-crystal data were collected with a Bruker AXS Smart 1000 area detector diffractometer, Mo Kα λ = 0.71073 Å. The unit cell parameters were obtained using 60 ω frames of 0.5° width and scanned from three different zones of the reciprocal lattice. Intensity data were integrated from several series of exposures frames (0.3° width) covering the sphere of reciprocal space.[29] An absorption correction was applied using the program SADABS[30] with min and max trasmission factors of 0.846 and 1.000 ($[Ni(Bz_2pipdt)(mnt)]$), 0.805 and 1.000 ($[Pd(Bz_2pipdt)(mnt)]$), and 0.640 and 1.000 ($[Pt(Bz_2pipdt)(mnt)]$). The structures were solved by direct methods (SIR97)[31] and refined on F^2 with full-matrix least-squares (SHELXL-97)[32] using the Wingx software package.[33] Non-hydrogen atoms were refined anisotropically for all compounds, and the hydrogen atoms were placed at their calculated positions. Graphical material was prepared with the ORTEP3 for Windows[34] and Mercury 2.0[35] programs. CCDC 820367−820369 contain the supplementary crystallographic data for this paper.

Computational Details. Ground-state electronic structure calculations of complexes **1**−**3** have been performed using density functional theory (DFT)[36] methods employing the GAUSSIAN 03[37] software packages. The functional used throughout this study was the B3LYP, consisting of a hybrid exchange functional as defined by Becke's three-parameter equation[38] and the Lee−Yang−Parr correlation functional.[39] The ground-state geometries were obtained in the gas phase by full geometry optimization, starting from structural data under no symmetry constraint. The final structures were found to be very close to the geometry imposed by point-group arguments, which is C_s for all. Thus, they were reoptimized in order to satisfy the higher symmetry expected.

The basis set employed for all nonmetal atoms was the well-known valence triple-ζ 6-311+G*.[40] In addition, we selected the Stuttgart−Dresden effective core potentials for the metal atoms in order to describe the core electrons.[41] ECPs were of the type 60MDF, 28MDF, and 10MHF for Pt, Pd, and Ni, respectively, unless otherwise stated. The latter were complemented by relative valence triple-ζ quality basis sets.[42] Furthermore, the converged wave functions were found free from internal instabilities. Percentage compositions of molecular orbitals were calculated using the AOMix suite of progams.[43]

Moreover, in our effort to fully understand formation of bonding interactions in the complexes under study we employed a charge decomposition analysis following the previously established methodology.[44,17a]

For uniformity purposes,[17f] basis sets of double-ζ quality were employed[45] but differences induced by the two basis sets employed were of only minor importance. Within this analysis special care was taken fot the produced wave functions of all fragments to be stable.

In order to model the compounds' interaction to a solvent's electric field, we employed the polarizable conductor calculation model (CPCM) as implemented in G03.[46] We set the α parameter at a value of 1.3 and used 80 tessarae per sphere, since a tighter option may result in charge penetration into the cavity. The 10 lowest singlet excited states of the closed-shell complexes were calculated within the TD-DFT formalism as implemented in Gaussian[47] in a DMSO-simulated electric field, while the percentage of different transitions contributing to a state were calculated with the aid of SWizard.[43,48]

The coupled perturbed Hartree−Fock method was employed to derive the compounds' hyperpolarizabilities.[49] Calculations were done to obtain $\beta(-\omega, \omega; 0)$ off resonance at 0.65 eV. Finally, the graphics presented here were drawn with the aid of ChemCraft.[50]

■ ASSOCIATED CONTENT

Supporting Information. Linear dependence of the peak currents from the square root of the voltage scan rate in the case of complex **2** (Figures S1−S4); calculated structures of **1**−**3** (Figure S5 and Table S1); contribution of different fragments to complexes valence orbitals in the gas phase and in the presence of a DMSO electric field (Tables S2 and S3); TD-DFT-calculated energies and compositions of the lowest lying singlet electronic transitions of **1**−**3** (Tables S4−S6); calculated hyperpolarizability values for **1**−**3** (Table S7). This material is available free of charge via the Internet at http://pubs.acs.org.

■ AUTHOR INFORMATION

Corresponding Author

*E-mail: deplano@unica.it; cmitsop@chem.uoa.gr.

■ ACKNOWLEDGMENT

This work has been performed through cooperation inside COST Action D35, WG11 "Multifunctional and Switchable Molecular Materials". D.E. is grateful to COST Action D35 for supporting STRM in Strasbourg. Università di Cagliari and the Special Research Account of NKUA are also acknowledged for financial support. Thanks are also due to Dr. M. Placidi, Jobin Yvon srl, for running Raman spectra.

■ REFERENCES

(1) Vogler, A.; Kunkely, H. *Angew. Chem., Int. Ed. Engl.* **1982**, *21*, 77.

(2) (a) Dithiolene Chemistry: Synthesis, Properties, and Applications. In *Progress in Inorganic Chemistry*; Cummings, S. D., Eisenberg, R., Stiefel, E. I., Eds.; Wiley: Chichester, 2004; Vol. 52, pp 315−367. (b) Cummings, S. D.; Eisenberg, R. *J. Am. Chem. Soc.* **1996**, *118*, 1949. (c) Cummings, S. D.; Cheng, L.-T.; Eisenberg, R. *Chem. Mater.* **1997**, *9*, 440. (d) Chen, C.-T.; Liao, S.-Y.; Lin, K.-J.; Chen, C.-H.; Lin, T-Y.J. *Inorg. Chem.* **1999**, *38*, 2734.

(3) Geary, E. A. M.; Yellowlees, L. J.; Jack, L. A.; Parson, S.; Hirata, N.; Durrant, J.; Robertson, N. *Inorg. Chem.* **2005**, *44*, 242.

(4) Zhang, J.; Du, P.; Schneider, J.; Jarosz, P.; Eisenberg, R. *J. Am. Chem. Soc.* **2007**, *129*, 7726.

(5) (a) Makedonas, C.; Mitsopoulou, C. A.; Lahoz, F. J.; Balana, A. I. *Inorg. Chem.* **2003**, *42*, 8853. (b) Mitsopoulou, C. A. *Coord. Chem. Rev.* **2010**, *254*, 1448.

(6) Base, K.; Tierney, M. T.; Fort, A.; Muller, J.; Grinstaff, M. W. *Inorg. Chem.* **1999**, *38*, 287.

(7) (a) Chen, C.-T.; Liao, S.-Y.; Lin, K.-J.; Lai, L.-L. *Adv. Mater.* **1998**, *3*, 335. (b) Bigoli, F.; Chen, C.-T.; Deplano, P.; Mercuri, M. L.; Pellinghelli, M. A.; Pilia, L.; Pintus, G.; Serpe, A.; Trogu, E. F. *Chem. Commun.* **2001**, 2246. (c) Deplano, P., Mercuri, M. L., Serpe, A., Pilia, L. In *Chemistry of Metal Enolates, Part 2, Patai Series*; Zabicky, J., Ed.; John Wiley & Sons, Ltd.: Chichester, U. K., 2009; p 879. (d) Deplano, P.; Pilia, L.; Espa, D.; Mercuri, M. L.; Serpe, A. *Coord. Chem. Rev.* **2010**, *254*, 1434.

(8) Deplano, P.; Marchiò, L.; Mercuri, M. L.; Pilia, L.; Pintus, G.; Serpe, A.; Yagubskii, E. B. *Monatsh. Chem.* **2009**, *140*, 775.

(9) Bigoli, F.; Deplano, P.; Mercuri, M. L.; Pellinghelli, M. A.; Pilia, L.; Pintus, G.; Serpe, A.; Trogu, E. F. *Inorg. Chem.* **2002**, *41*, 5241.

(10) (a) Pilia, L.; Artizzu, F.; Faulmann, C.; Mercuri, M. L.; Serpe, A.; Deplano, P. *Inorg. Chem. Commun.* **2009**, *12*, 490. (b) Papavassiliou, C.; Anyfantis, G. C.; Terzis, A.; Psycharis, V.; Kyritsis, P.; Paraskevopoulou, P. *Z. Naturforsch.* **2008**, *63b*, 1377. (c) Papavassiliu, G. C.; Anyfantis, G. C. *Z. Naturforsch.* **2005**, *60b*, 811.

(11) Espa, D.; Pilia, L.; Marchio, L.; Mercuri, M. L.; Serpe, A.; Barsella, A.; Fort, A.; Dalgleish, S. J.; Robertson, N.; Deplano, P. *Inorg. Chem.* **2011**, *50*, 2058–2060.

(12) $[Pd(CH_3CN)Cl_2]$ is provided by Sigma Aldrich; $[Pt(DMSO)_2Cl_2]$ is prepared according to the following: Kukushkin, Y. N.; Viez'menskii, Y. E.; Zorina, L. I. *Russ. J. Inorg. Chem.* **1968**, 835.

(13) Mahadevan, C.; Seshasayee, M.; Radha, A.; Manoharan, P. T. *Acta Crystallogr.* **1984**, *C40*, 2032.

(14) (a) Schlapfer, W.; Nakamoto, K. *Inorg. Chem.* **1975**, *14*, 1338. (b) Wootton, J. L.; Zink, J. I. *J. Phys. Chem.* **1995**, *99*, 7251. (c) Pokhodnya, K. I.; Faulmann, C.; Malfant, I.; Andreu-Solano, R.; Cassoux, P.; Mlayah, A.; Smirnov, D.; Leotin, J. *Synth. Met.* 1999, *103*, 2016. (d) Wang, H. H.; Fox, S. B.; Yagubskii, E. B.; Kushch, L. A.; Kotov, A. I.; Whangbo, M.-H. *J. Am. Chem. Soc.* **1997**, *119*, 7601.

(15) (a) Nishio, M. *Cryst. Eng. Commun.* **2004**, *6*, 130. (b) Nishio, M.; Umezawa, Y.; Honda, K.; Tsuboyama, S.; Suezawa, H. *Cryst. Eng. Commun.* **2009**, *11*, 1757.

(16) Cariati, E.: Pizzotti, M.; Roberto, D.; Tessore, F.; Ugo, R. *Coord. Chem. Rev.* **2006**, *250*, 1210 and references therein.

(17) (a) Makedonas, C.; Mitsopoulou, C. A. *Eur. J. Inorg. Chem.* **2007**, 110. (b) Makedonas, C.; Mitsopoulou, C. A. *Spectrochim. Acta, Part A* **2006**, *64*, 918. (c) Makedonas, C.; Mitsopoulou, C. A. *Eur. J. Inorg. Chem.* **2006**, 2460. (d) Makedonas, C.; Mitsopoulou, C. A. *Eur. J. Inorg. Chem.* **2006**, 590. (e) Makedonas, C.; Mitsopoulou, C. A. *Inorg. Chim. Acta* **2007**, *360*, 3997. (f) Makedonas, C.; Mitsopoulou, C. A. *Eur. J. Inorg. Chem.* **2007**, 4176. (g) Mitsopoulou, C. A.; Dagas, C. E.; Makedonas, C. *Inorg. Chim. Acta* **2008**, *361*, 1973. (h) Mitsopoulou, C. A.; Dagas, C. E.; Makedonas, C. *J. Inorg. Biochem.* **2008**, *102*, 77.

(18) (a) Curreli, S.; Deplano, P.; Faulmann, C.; Ienco, A.; Mealli, C.; Mercuri, M. L.; Pilia, L.; Pintus, G.; Serpe, A.; Trogu, E. F. *Inorg. Chem.* **2004**, *43*, 5069. (b) Bigoli, F.; Cassoux, P.; Deplano, P.; Mercuri, M. L.; Pellinghelli, M. A.; Pintus, G.; Serpe, A.; Trogu, E. F. *J. Chem. Soc., Dalton Trans.* **2000**, 4639.

(19) Koch, W.; Holthausen, M. C. *A Chemist's Guide to Density Functional Theory*; Wiley-VCH Verlag GmbH: Weinheim, 2000.

(20) Li, J.; Noodleman, L.; Case, D. A. In *Inorganic Electronic Stucture and Spectroscopy*; Solomon, E. I., Lever, A. B. P., Eds.; John Wiley & Sons: New York, 1999; Vol. 1, pp 661−724.

(21) (a) Szylagyi, R. K.; Lim, B. S.; Glaser, T.; Holm, R. H.; Hedman, B.; Hodgson, K. O.; Solomon, E. I. *J. Am. Chem. Soc.* **2003**, *125*, 9158. (b) Solomon, E. I.; Hedman, B.; Hodgson, K. O.; Dey, A.; Szylagyi, R. K. *Coord. Chem. Rev.* **2005**, *249*, 97. (c) Bruno, G.; Almeida, M.; Artizzu, F.; Dias, J. C.; Mercuri, M. L.; Pilia, L.; Rovira, C.; Ribas, X.; Serpe, A.; Deplano, P. *Dalton. Trans.* **2010**, *39*, 4566.

(22) Juris, A.; Deplano, P. et al. Unpublished results.

(23) (a) Zuleta, J. A.; Burberry, M. S.; Eisenberg, R. *Coord. Chem. Rev.* **1990**, *97*, 47. (b) Harvey, P. D.; Eisenberg, R. *Inorg. Chem.* **1992**, *31*, 2396.

(24) Casida, M. E.; Jamorski, C.; Casida, K. C.; Salahub, D. R. *J. Chem. Phys.* **1998**, *108*, 4439.
(25) (a) Romaniello, P.; Lelj, F. *J. Mol. Struct. (THEOCHEM)* **2003**, *636*, 23–37. (b) Romaniello, P.; Lelj, F. *J. Mol. Struct. (THEOCHEM)* **2003**, *372*, 51.
(26) Romaniello, P.; D'Andria M.C. Lelj, F. *J. Phys. Chem. A* **2010**, *114*, 5838.
(27) Isaksson, R.; Liljefors, T.; Sandstrom, J. *J. Chem. Res., Miniprint* **1981**, 664.
(28) (a) Bähr, G.; Schleitzer, G. *Ber* **1955**, *88*, 1771. (b) Bähr, G.; Schleitzer, G. *Ber* **1957**, *90*, 438. (c) Bähr, G. *Angew. Chem.* **1953**, *68*, 525.
(29) *SMART (control) and SAINT (integration) software for CCD systems*; Bruker AXS: Madison, WI, 1994.
(30) *Area-Detector Absorption Correction*; Siemens Industrial Automation, Inc.: Madison, WI, 1996.
(31) Altomare, A.; Burla, M. C.; Camalli, M.; Cascarano, G. L.; Giacovazzo, C.; Guagliardi, A.; Moliterni, A. G. G.; Polidori, G.; Spagna, R. *J. Appl. Crystallogr.* **1999**, *32*, 115.
(32) Sheldrick, G. M. *SHELX97, Programs for Crystal Structure Analysis (Release 97-2)*; University of Göttingen, Germany, 1997.
(33) Farrugia, L. J. *J. Appl. Crystallogr.* **1999**, *32*, 837.
(34) Farrugia, L. J. *J. Appl. Crystallogr.* **1997**, *30*, 568.
(35) Macrae, C. F.; Edgington, P. R.; McCabe, P.; Pidcock, E.; Shields, G. P.; Taylor, R.; Towler, M.; van de Streek, J. *J. Appl. Crystallogr.* **2006**, *39*, 453.
(36) Parr, R. G.; Yang, W. *Density Functional Theory of Atoms and Molecules*; Oxford University Press: Oxford, 1989.
(37) Frisch, M. J.; Schlegel, G. W. T.; Scuseria, H. B.; Robb, G. E.; Cheeseman, M. A.; Montgomery, J. R., Jr., Vreven, J. A.; Kudin, T.; Burant, K. N.; Millam, J. C.; Iyengar, J. M.; Tomasi, S. S.; Barone, J.; Mennucci, V.; Cossi, B.; Scalmani, M.; Rega, G.; Petersson, N.; Nakatsuji, G. A.; Hada, H.; Ehara, M.M.; Toyota, K.; Fukuda, R.; Hasegawa, J.; Ishida, M.; Nakajima, T.; Honda, Y.; Kitao, O.; Nakai, H.; Klene, M.; Li, X.; Knox, J. E.; Hratchian, H. P.; Cross, J. B.; Adamo, C.; Jaramillo, J.; Gomperts, R.; Stratmann, R. E.; Yazyev, O.; Austin, A. J.; Cammi, R.; Pomelli, C.; Ochterski, J. W.; Ayala, P. Y.; Morokuma, K.; Voth, G. A.; Salvador, P.; Dannenberg, J. J.; Zakrzewski, V. G.; Dapprich, S.; Daniels, A. D.; Strain, M. C.; Farkas, O.; Malick, D. K.; Rabuck, A. D.; Raghavachari, K.; Foresman, J. B.; Ortiz, J. V.; Cui, Q.; Baboul, A. G.; Clifford, S.; Cioslowski, J.; Stefanov, B. B.; Liu, G.; Liashenko, A.; Piskorz, P.; Komaromi, I.; Martin, R. L.; Fox, D. J.; Keith, T.; Al-Laham, M. A.; Peng, C. Y.; Nanayakkara, A.; Challacombe, M.; Gill, P. M. W.; Johnson, B.; Chen, W.; Wong, M. W.; Gonzalez, C.; Pople, J. A. *Gaussian 03*, revision B.1; Gaussian, Inc.: Pittsburgh, PA, 2003.
(38) Becke, A. D. *J. Chem. Phys.* **1993**, *98*, 5648.
(39) Lee, C.; Yang, W.; Parr, R. G. *Phys. Rev. B* **1988**, *37*, 785.
(40) (a) Krishnan, R.; Binkley, J. S.; Seeger, R.; Pople, J. A. *J. Chem. Phys.* **1980**, *72*, 650–654. (b) McLean, A. D.; Chandler, G. S. *J. Chem. Phys.* **1980**, *72*, 5639.
(41) Andrae, D.; Häußermann, U.; Dolg, M.; Stoll, H.; Preuß, H. *Theor. Chim. Acta* **1990**, *77*, 123.
(42) (a) Dolg, M.; Wetig, U.; Stoll, H.; Preuss, H. *J. Chem. Phys.* **1987**, *86*, 866. (b) Figgen, D.; Peterson, K. A.; Dolg, M.; Stoll, H. *J. Chem. Phys.* **2009**, *130*, 164108. (c) Martin, J. M. L.; Sunderman, A. *J. Chem. Phys.* **2001**, *114*, 3408. (d) Peterson, K. A.; Figgen, D.; Dolg, M.; Stoll, H. *J. Chem. Phys.* **2007**, *126*, 124101.
(43) (a) Gorelsky, S. I. *AOMix and AOMix-S programs*, revision 6.46; http://www.sg-chem.net/. (b) Gorelsky, S. I.; Lever, A. B. P. *J. Organomet. Chem.* **2001**, *635*, 187.
(44) (a) Gorelsky, S. I.; Ghosh, S.; Solomon, E. I. *J. Am. Chem. Soc.* **2006**, *128*, 278. (b) Gorelsky, S. I.; Solomon, E. I. *Theor. Chem. Acc.* **2008**, *119*, 57.
(45) (a) Hay, P. J.; Wadt, W. R. *J. Chem. Phys.* **1985**, *82*, 270. (b) Dunning, T. H. J.; Hay, P. J. In *Modern Theoretical Chemistry*; Schaefer, H. F., I, Ed.; Plenum Press: New York, 1976; Vol. 3.
(46) (a) Barone, V.; Cossi, M. *J. Phys. Chem. A* **1998**, *102*, 1995. (b) Cossi, M.; Rega, N.; Scalmani, G.; Barone, V. *J. Comput. Chem.* **2003**, *24*, 669.
(47) Stratmann, R. E.; Scuseria, G. E.; Frisch, M. J. *J. Chem. Phys.* **1998**, *109*, 8218.
(48) Gorelsky, S. I. *SWizard program*, revision 4.6; http://www.sg-chem.net/
(49) (a) Gerratt, J.; Mills, I. M. *J. Chem. Phys.* **1968**, *49*, 1719. (b) Pulay, P. *J. Chem. Phys.* **1983**, *78*, 5043. (c) McWeeny, R. *Rev. Mod. Phys.* **1960**, *32*, 335.
(50) Zhurko, G. A.; Zhurko, D. A. *ChemCraft, Tool for treatment of the chemical data*, version 1.6; www.chemcraftprog.com